Available online at www.sciencedirect.com
ScienceDirect
Journal of Catalysis 247 (2007) 356–367
JOURNAL OF CATALYSIS
www.elsevier.com/locate/jcat

Cobalt-based catalysts supported on titania and zirconia for the oxidation of nitric oxide to nitrogen dioxide

Matthew M. Yung, Erik M. Holmgreen, Umit S. Ozkan *

Department of Chemical and Biomolecular Engineering, The Ohio State University, 140 W. 19th Avenue, Columbus, OH 43210, USA

Received 28 November 2006; revised 3 February 2007; accepted 8 February 2007

Available online 23 March 2007

Abstract

Cobalt-based catalysts supported on TiO_2 and ZrO_2 were studied for the oxidation of NO to NO_2 in excess oxygen. NO oxidation was studied as the first step in a two-step catalytic scheme where NO is oxidized to NO_2 and in turn NO_2 is reduced with CH_4 to N_2 under lean conditions. Catalysts were prepared by sol–gel (SG) and incipient-wetness impregnation (IWI) techniques and characterized by temperature-programmed reduction (TPR), X-ray photoelectron spectroscopy (XPS), X-ray diffraction (XRD), laser Raman spectroscopy (LRS), and diffuse reflectance Fourier transform infrared spectroscopy (DRIFTS). It was found the nature of the support, the synthesis technique, and the pretreatment conditions affect the catalytic activity. 10% Co/ZrO_2 catalysts prepared by IWI were found to be most active among the catalysts tested, giving the highest NO uptake capacity and the highest turnover frequency (TOF) based on NO adsorption sites. Tests with bulk Co_3O_4 also showed significant NO oxidation activity.

Keywords: NO oxidation; NO_2; NO_x; Cobalt; Co_3O_4; TiO_2; ZrO_2; XPS; TPR; Raman; DRIFTS

1. Introduction

Nitrogen oxides are known to be associated with several environmental and health hazards, including smog, acid rain, and ground-level ozone formation. Due to the increasingly stringent regulations on nitrogen oxide emissions, development of methods to decrease NO_x emissions has been an active research area [1]. Currently, ammonia selective catalytic reduction (SCR) is a popular choice for NO_x reduction for stationary applications [2]. This technology can be used in both lean and rich conditions. Because of the cost and safety hazards associated with ammonia SCR installations, and due to the presence of unburned hydrocarbons in the exhaust of lean-burning engines, the use of hydrocarbons as a NO_x reduction agent is an attractive alternative. Thus, SCR of NO_x using methane and other hydrocarbons has received much research attention [3–19]. Lean-burning natural gas and diesel engines are becoming increasingly popular choices for stationary power generation and mobile applications due to their high operating efficiencies and relatively low emissions. A challenge to these lean-burning engines, however, is the development of a catalyst that can reduce NO_x species in the highly oxidizing conditions by avoiding the undesired reactions between the hydrocarbons and molecular oxygen [2].

For the SCR of NO with hydrocarbons, ion-exchanged zeolites, such as Cu-, Fe-, Pt-, Co-, Ga-, Ce-, and H-exchanged zeolites, have been shown to be active [7–14]. Supported noble metals also have been researched. Cu-ZSM-5 and Pt/Al_2O_3 are among the most widely studied metal-exchanged zeolite and supported noble metal catalysts for the NO SCR with hydrocarbons [7]. Although there is debate regarding the mechanisms involved in NO SCR with hydrocarbons, it is often proposed that NO is first oxidized to NO_2, which subsequently reacts with the hydrocarbon and is reduced [20–22]. A study by Meunier and Ross [23] compared conversions of NO and NO_2 over silver-based catalysts with propane and found superior activity for NO_2 reduction with hydrocarbons compared with that for NO, supporting the idea that NO_2 is a key reaction intermediate [23–29]. Because NO_2 is more "oxidized" than NO, it can be

* Corresponding author. Fax: +1 614 292 3769.
E-mail address: ozkan.1@osu.edu (U.S. Ozkan).

0021-9517/$ – see front matter
doi:10.1016/j.jcat.2007.02.020

reduced more readily, making it able to more favorably compete with O_2 for reaction with the reducing agent.

Oxygen reportedly shows a promotional effect on the rate of NO reduction with hydrocarbons, purportedly due to a bifunctional catalytic mechanism on Cu-ZSM-5 [7]. Other studies have also proposed bifunctional catalysts for the NO SCR with hydrocarbons, with some sites responsible for NO oxidation and other sites responsible for the reduction of NO_2, and observed superior N_2 yields when NO_2 rather than NO was reduced [7,20,21,29–31]. A study on Co-mordenite catalysts suggested that high metal loadings promote the oxidation of NO to NO_2, which can enhance the overall N_2 formation [21]. Because NO_2 has been proposed as a reaction intermediate, the study of NO oxidation can be found in the NO SCR literature as well as in some direct studies of NO oxidation [25–28]. Studies on Ag, Co, and Pt catalysts have shown that they can exhibit significant oxidation activity [5,32–35]. A study by Despres et al. examined direct NO oxidation on Pt/SiO_2 and found that the NO conversion was heavily dependent upon reaction conditions and that the oxidizing conditions and exposure to NO_2 led to formation of a thin layer of platinum oxide that caused a strong and persistent decrease in activity. A similar observation was also reported for Pt/Al_2O_3 and Pt/ZrO_2 [22]. To avoid the potential problem of activity losses in strongly oxidizing environments, inexpensive alternatives to Pt, such as cobalt, are under investigation. A study of NO_2 reduction with methane over Co-ZSM-5 proposed that the support contained the active sites for NO_2 reduction, while the Co sites reoxidized NO formed from high-temperature decomposition of NO_2 [32]. In addition to NO_x catalysis, cobalt catalysts on oxide supports, especially TiO_2, have been studied for a various reactions, including Fischer–Tropsch synthesis [36–39], oxidation reactions [40–42], and oxidative dehydrogenation [43,44]. These studies found the presence of Co_3O_4 has been observed and noted its high activity for oxidation reactions.

We have previously discussed the development of a two-step catalytic system for the reduction of NO with CH_4 under lean conditions and reported on the NO_2 reduction with CH_4 over Pd-based catalysts [45–48]. The two-step approach aims to develop separate catalytic systems for the oxidation of NO to NO_2, as well as for the reduction of NO_2 with CH_4, to take advantage of the stronger oxidizing potential of NO_2. In the proposed scheme, unburned methane in the exhaust would be used as the reducing agent, without the need for any additional fuel injection. The oxidation and reduction catalysts can be physically mixed together. Although the exothermic oxidation of NO to NO_2 is thermodynamically limited at high temperatures [22], in the combined two-step scheme, NO_2 is continuously removed from the system by reduction to N_2, shifting the NO oxidation reaction to the right. Experiments that we conducted have verified the benefit of the two-step system, giving higher N_2 yields using the two-step reduction of NO than using the single-step reduction of NO_2. In addition, NO_2 that was partially reduced to NO can be reoxidized in a two-step scheme.

As was expected, methane conversion was higher over the mixed-bed catalyst than over the reduction catalyst, especially at 350 °C and higher. Whereas the experiments using the mixture of oxidation and reduction catalysts caused increased conversion of methane, the NO_x conversion to N_2 was not hindered [47]. Although the typical operating temperatures for the NO_x reduction reaction are higher than the point at which many of the experiments in this study achieved thermodynamic equilibrium, it is still important to study catalyst activity at lower temperatures to minimize the required catalyst mass/cost. In addition, comparing the N_2 yields obtained from two-stage experiments with different oxidation catalysts showed benefits for the more active oxidation catalyst even at high temperatures, due to its ability to rapidly oxidize NO as NO_2 is removed by either full or partial reduction [47]. This paper addresses the oxidation of NO to NO_2 over metal-oxide-supported cobalt catalysts in excess oxygen conditions.

2. Experimental

2.1. Catalyst synthesis

Catalysts were prepared by incipient-wetness impregnation (IWI) and modified sol–gel (SG) techniques. Catalyst loadings are calculated and designated as wt%. Aqueous $Co(NO_3)_2{\cdot}6H_2O$ (Aldrich) was used to impregnate commercial TiO_2 (lot 2001250711) and ZrO_2 (lot 2000920047) supports, provided by Saint Gobain. The catalysts were dried in air at 110 °C overnight, then heated to their calcination temperature at a rate 10 °C/min and held there for 3 h. Sol–gel catalysts used alkoxide precursors, titanium isopropoxide (Aldrich), and zirconium propoxide (Aldrich), which were added to an isopropyl alcohol solvent solution to obtain a concentration of 0.2 M. An above-stoichiometric ratio of water to alkoxide (7:1) was used to increase the rate of hydrolysis. $Co(NO_3)_2{\cdot}6H_2O$ (Aldrich) was dissolved in the water used for the hydrolysis step. The aqueous solution was added to the stirred alkoxide mixture at a rate of 0.2 mL/min by a syringe pump. The sample was dried in air overnight and then calcined in air for 3 h. Catalysts are designated by appending the synthesis technique and calcination temperature to the composition.

2.2. Catalyst activity testing

Steady-state reaction experiments were performed in a stainless steel fixed-bed flow reactor (1/4 inch o.d.). Unless specified otherwise, 200 mg of catalyst was used and held in place by quartz wool plugs, with the temperature measured by an Omega K-type thermocouple in direct contact with the downstream quartz plug. The feed consisted of NO (1000 ppm) and O_2 (10%) in a balance of He. For runs that contained water in the feed, the water concentration was 10%, and lines downstream of the bubbler were heated to prevent condensation. The feed flow rate was 45 cm^3(STP)/min, corresponding to a typical space velocity of 35,000/h. Samples were pretreated in 10% O_2 at 300 °C for 30 min. On-line analysis of the feed and effluent gas streams was performed using a gas chromatograph (Varian Micro-GC CP4900) with a molecular sieve and Porapaq Q columns and a chemiluminescence NO–NO_2–NO_x analyzer

Table 1
BET surface areas of the unloaded supports and the prepared catalysts

Catalyst composition	Synthesis technique	Calcination temperature (°C)	Surface area (m^2/g)
10% Co/TiO_2	Sol–gel	300	278
10% Co/TiO_2	Sol–gel	400	95
10% Co/TiO_2	Sol–gel	500	25
10% Co/TiO_2	Sol–gel	600	5
TiO_2 powder	n/a	550	91
10% Co/TiO_2	IWI	300	65
10% Co/TiO_2	IWI	400	64
10% Co/TiO_2	IWI	500	52
10% Co/TiO_2	IWI	600	31
10% Co/ZrO_2	Sol–gel	350	37
ZrO_2 powder	n/a	500	48
10% Co/ZrO_2	IWI	300	43
10% Co/ZrO_2	IWI	400	42
10% Co/ZrO_2	IWI	500	41
10% Co/ZrO_2	IWI	600	37
1% Co/ZrO_2	IWI	300	47
5% Co/ZrO_2	IWI	300	48
15% Co/ZrO_2	IWI	300	39
Bulk Co_3O_4 powder	n/a	550	15

(Thermo Environmental Instruments 42H). For runs that contained water, the product stream was sent through a condenser to condense the water, and a Drierite column was used on the split injection line upstream of the GC to eliminate the remaining water in the stream. Yields of NO_2, N_2, and N_2O are defined based on the NO_x in the feed using the relationship

$$\text{yield of product A} = (\text{moles of A produced}) \times \frac{\#\text{ of N atoms per molecule of A}}{\text{moles of NO fed}}.$$

2.3. Catalyst characterization

The BET surface area for catalysts was determined using N_2 physisorption on a Micrometrics ASAP 2010 at 77 K. Table 1 gives the BET surface area, calcination temperature, and synthesis technique of the catalysts examined in this study. In situ X-ray diffraction (XRD) patterns of powdered samples were obtained using a Bruker D8 Advance X-ray diffractometer equipped with a CuK_α source with wavelength 1.54 Å. The experiments were conducted by increasing the sample temperature in 50 °C increments at a rate of 5 °C/min. At each temperature, the sample was held for 10 min before the diffraction pattern was taken. During the calcination experiments, an air stream with a constant flow rate of 10 cm^3/min was passed over the sample.

Temperature-programmed reduction (TPR) experiments were performed on an in-house-constructed system equipped with a TCD detector to measure H_2 consumption. A water trap removed moisture from the TPR effluent stream before the TCD. The reduction of CuO was used to calibrate the TCD signal for H_2 consumption. Reported average oxidation states quantify the ratio of H_2 consumption to cobalt content during the TPR experiments and reflect the difference between the initial and final oxidation states. Quartz U-tube reactors were generally loaded with 100 mg of sample, and catalysts were pretreated by calcination in 20% O_2/N_2 at 300 °C for 30 min, then cooled to room temperature. The TPR was performed using 30 cm^3/min of 10% H_2/N_2, with the temperature ramped from 25 to 800 °C at 10 °C/min. TPR experiments were repeated using an on-line mass spectrometer (Cirrus RGA) to detect any species eluting from the surface.

X-ray photoelectron spectroscopy (XPS) experiments were performed on an AXIS Ultra instrument using a monochromatic aluminum X-ray source. Samples were degassed overnight to a pressure of 10^{-6} Torr before being transferred to the analysis chamber, operating at a vacuum of 10^{-9} Torr. Charge-shift corrections were performed based on the standard location of the carbon 1s peak, 284.5 eV. Raman spectra were obtained on powdered samples at room temperature using a Horiba Jobin-Yvon LabRam HR800 spectrometer with a 50× microprobe in the backscattering geometry and a 514.5-nm argon ion laser (Coherent Innova I70C-5).

Diffuse reflectance Fourier transform infrared measurements (DRIFTS) were performed with a Thermo Nicolet 6700 spectrometer with a KBr beam-splitter and a liquid N_2-cooled MCT detector at spectral resolution of 4 cm^{-1} (500 scans). Samples were pretreated at 400 °C in 5% O_2/He for 30 min at a flow rate of 25 mL/min, and backgrounds were taken during cooling under He flow. Adsorption of either NO or NO_2 at 5100 ppm in balance He was performed for 30 min at 50 °C, after which the sample was then flushed with He for 10 min. Spectra were acquired after 10 min at 50 °C increments.

NO uptake measurements were performed through a pulsed-chemisorption technique using on-line mass spectrometry (Cirrus RGA). The measurements were performed at 50 °C using 5-mL pulses of 5100 ppm NO in helium.

3. Results

3.1. Steady-state reaction experiments

Fig. 1a shows the conversion of NO to NO_2 (i.e., NO_2 yield) obtained over a series of 10% Co/TiO_2 sol–gel catalysts calcined at various temperatures. For reference, the thermodynamic equilibrium for NO conversion to NO_2 is also shown in all activity figures for the given reaction conditions. As was expected, the NO_2 yield became equilibrium-limited, rather than kinetically limited, at higher reaction temperatures. Above temperatures at which the equilibrium curve was reached, the catalyst activity in each experiment closely followed the equilibrium NO_2 yield. The most active sample in this series was 10% Co/TiO_2 SG 400, which reached equilibrium at 300 °C, corresponding to a NO_2 yield of 84%. Samples calcined at 500 and 600 °C had lower activity compared with the sample calcined at 400 °C, and these samples required higher temperatures to reach the equilibrium curve. The sample calcined at 300 °C had a maximum NO_2 yield of 48% at 400 °C. It is interesting to note that the sol–gel sample calcined at 300 °C did not follow the trend toward decreased activity based on increasing calcination temperature, because it had lower activity than the catalyst

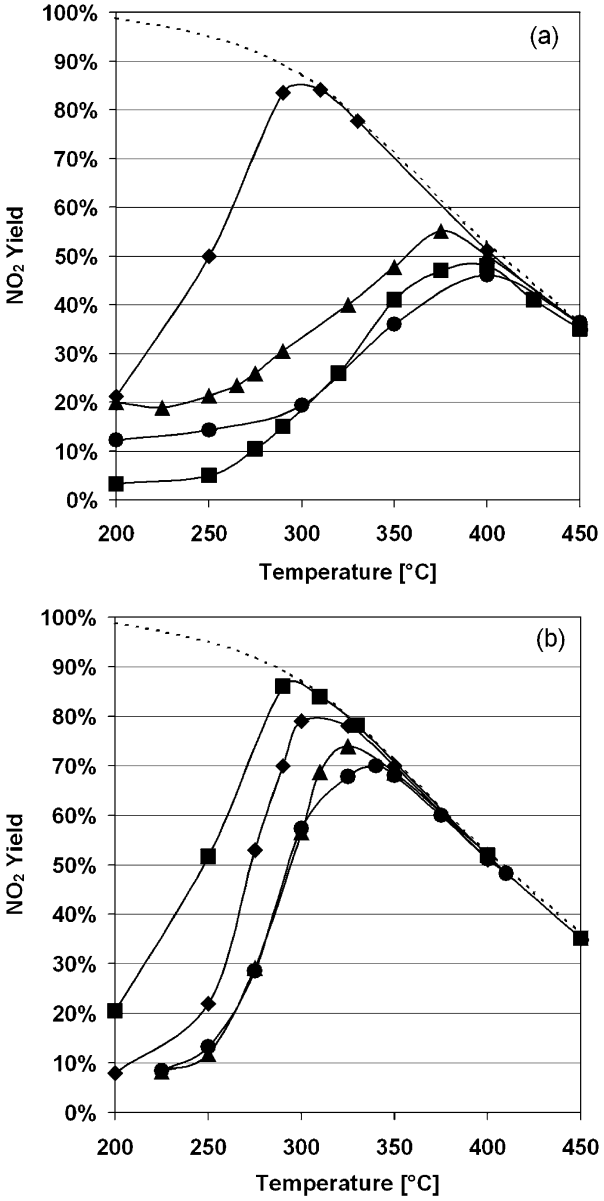

Fig. 1. Comparison of NO oxidation activities of 10% Co/TiO_2 catalysts calcined at (■) 300, (◆) 400, (▲) 500, and (●) 600 °C. Synthesis method: (a) sol–gel; (b) incipient-wetness.

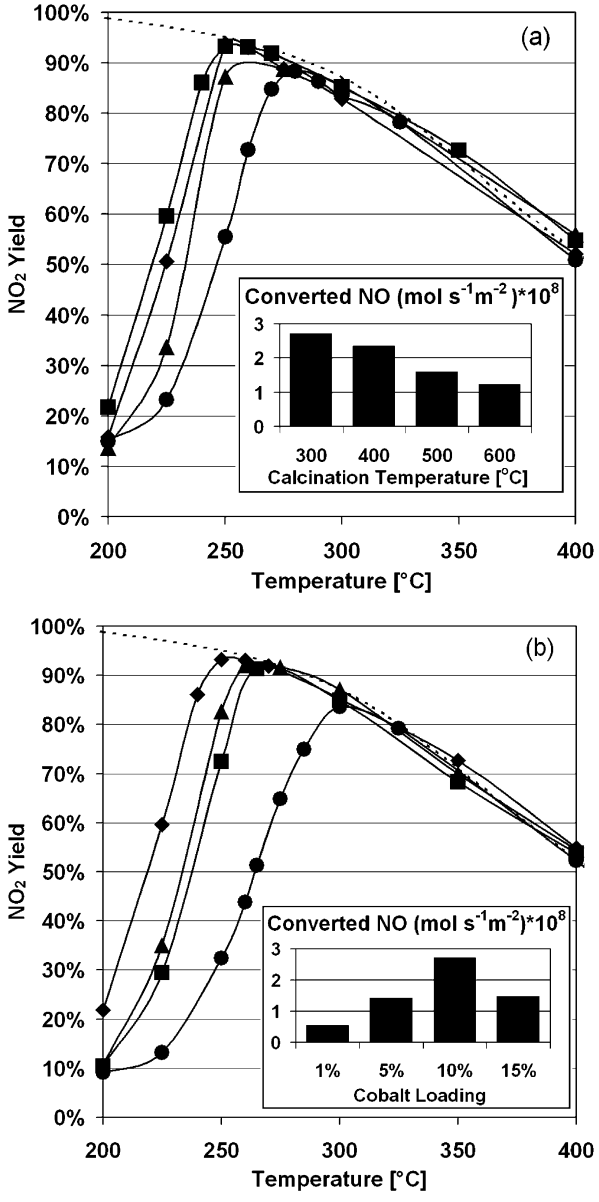

Fig. 2. (a) Comparison of activities of 10% Co/ZrO_2 IWI catalysts calcined at (■) 300, (◆) 400, (▲) 500, and (●) 600 °C. Inset (a): NO conversion rates at 225 °C. (b) Comparison of activities of Co/ZrO_2 IWI300 catalysts at various cobalt loadings: (■) 15, (◆) 10, (▲) 5, and (●) 1%. Inset (b): NO conversion rates at 225 °C.

that was calcined at 400 °C, despite having a higher surface area. XRD results showed that the sample calcined at 300 °C was amorphous, lacking TiO_2 crystallinity, which may in part explain the different behavior in activity.

Reaction results for the NO oxidation performed over 10% Co/TiO_2 IWI catalysts calcined at various temperatures are shown in Fig. 1b. The 10% Co/TiO_2 IWI 300 catalyst was the most active of this series and gave a substantially higher NO_2 yield at 250 °C than the samples at other calcination temperatures. The activity decreased with increasing calcination temperature. The 10% Co/TiO_2 IWI samples calcined at 400, 500, and 600 °C required progressively higher temperatures to reach equilibrium conversion. In the kinetically controlled region below 300 °C, the activity differences cannot be explained solely by the differences in surface area, because the catalysts calcined at 300 and 400 °C had identical surface areas. Comparison of the activity and surface area differences between the sol–gel and IWI preparations indicates that preparation technique also affected the NO oxidation activity.

The NO oxidation activities of 10% Co/ZrO_2 IWI catalysts calcined at various temperatures are shown in Fig. 2a. As was previously noted for the TiO_2-supported cobalt catalysts, we again observed the general trend of decreased activity and surface area with increasing calcination temperature, although this effect was much less pronounced in the ZrO_2-supported samples. The ZrO_2-supported catalysts showed both higher activity and better thermal stability than the TiO_2-supported catalysts. The 10% Co/ZrO_2 IWI catalysts calcined at 300 and 400 °C showed the highest activity from this series. Comparison of the

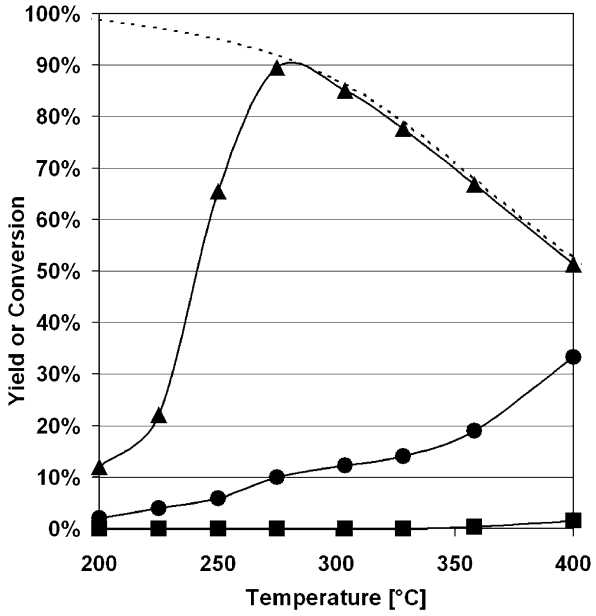

Fig. 3. Activity of 10% Co/ZrO_2 IWI in the presence of methane: (▲) NO_2 yield, (●) CH_4 conversion, and (■) N_2 yield.

NO_2 yields at 225 °C clearly shows the decreased activity with increasing calcination temperature. A comparison of the conversion rates at 225 °C, normalized with respect to surface area, is presented in the inset for the catalysts calcined at different temperatures. This comparison shows that the effect of calcination temperature on activity displays the same trend as the comparison made using equal catalyst weights.

Fig. 2b shows the effect of metal loading on the activity of Co/ZrO_2 IWI catalysts calcined at 300 °C. The 1% Co/ZrO_2 sample showed considerably lower activity than the higher metal loadings and did not reach the equilibrium curve until 300 °C. The inset compares the conversion rates normalized with respect to surface area at 225 °C; this comparison also shows that 10% loading is the optimum value among the tested loading levels. One additional 10% Co/ZrO_2 catalyst was also prepared by the sol–gel technique and calcined at 350°C. Reaction testing of 10% Co/ZrO_2 SG350 showed that it was less active than the ZrO_2 IWI catalysts, with a 17% NO_2 yield at 250 °C.

Because these catalysts are envisioned to be part of a two-step reduction scheme in which NO is oxidized to NO_2 over the Co-based catalysts, and NO_2 will be reduced to N_2 over a reduction catalyst using methane, they were also tested in the presence of CH_4. Fig. 3 shows the NO and N_2 yields and CH_4 conversion data taken over the 10% Co/ZrO_2 IWI300 catalyst. The feed composition was 3000 ppm of CH_4, 1000 ppm of NO, and 10% O_2. The conversion of NO to NO_2 was slightly lower, but equilibrium was reached at 275 °C, providing a maximum NO_2 yield of 90%. The catalyst had very low activity for the reduction of NO to N_2, but activity for the oxidation of CH_4 to CO_2 was observed. In the combined two-stage reduction of NO_x, the NO oxidation and CH_4 conversion must be balanced to avoid elimination of the reducing agent by oxidation with molecular oxygen [47]. Activity measurements performed with

Table 2
NO conversion rates at 225 and 250 °C. Units of $(mol/(m^2\ s)) \times 10^8$

Temperature (°C)	10% Co/ZrO_2 SG	10% Co/TiO_2 SG	10% Co/TiO_2 IWI	10% Co/ZrO_2 IWI
225	0.18	0.77	1.22	2.72
250	0.91	1.37	1.92	3.92

Table 3
NO uptake and turnover frequencies

Temperature (°C)	10% Co/ZrO_2 SG	10% Co/TiO_2 SG	10% Co/TiO_2 IWI	10% Co/ZrO_2 IWI
	NO uptake at 50 °C (μmol/m^2)			
	0.54	0.40	0.53	1.16
	Turnover frequency (s^{-1})			
225	3.4E−03	1.9E−02	2.0E−02	2.3E−02
250	1.7E−02	2.6E−02	3.0E−02	3.7E−02

10% H_2O over the 10% Co/ZrO_2 IWI and 10% Co/TiO_2 IWI catalysts did not show any major inhibition effects of water on the catalytic performance.

Reactions using amounts of catalyst to obtain equal surface areas in the reactor (8.6 m^2) were also performed on the most active catalyst from each series: 10% Co/ZrO_2 SG350, 10% Co/TiO_2 SG400, 10% Co/TiO_2 IWI300, and 10% Co/ZrO_2 IWI300. A comparison of the NO conversion rates at 225 and 250 °C during these experiments is presented in Table 2. The type of catalyst support had a significant effect on the rate of reaction, again with the highest rate of reaction seen on the Co/ZrO_2 IWI catalyst.

In an effort to compare the catalysts based on TOFs, NO chemisorption uptake was quantified as representative of the NO adsorption sites. The NO uptake capacities and TOFs calculated as (mol NO converted/time)/(mol NO chemisorbed) are presented in Table 3. The bare supports, ZrO_2 and TiO_2, had no measurable NO uptake. These findings are noteworthy in two respects. Both the type of support and the synthesis technique play major roles in determining the site density for NO adsorption, with Co/ZrO_2 IWI catalysts having the highest uptake capacity. But comparing TOF values reveals differences, with the catalyst with the highest conversion rate based on equal surface area measurement also showing the highest TOF. Although the differences in TOF values are not as pronounced as the difference in conversion rates based on the surface area, the fact that TOF values are not equal suggests a difference in the intrinsic activity of the sites, depending on the support and the synthesis techniques used.

3.2. TPR

TPR was performed on the 10% Co/TiO_2 sol–gel, 10% Co/TiO_2 IWI, and 10% Co/ZrO_2 IWI catalyst series to compare the effect of calcination temperature and support choice on the reducibility of the supported Co. Fig. 4a shows TPR for the 10% Co/TiO_2 sol–gel series, as well as Co_3O_4 and CoO for reference. The SG300 and SG400 samples showed broad reduction peaks beginning between 400 and 450 °C and ending between

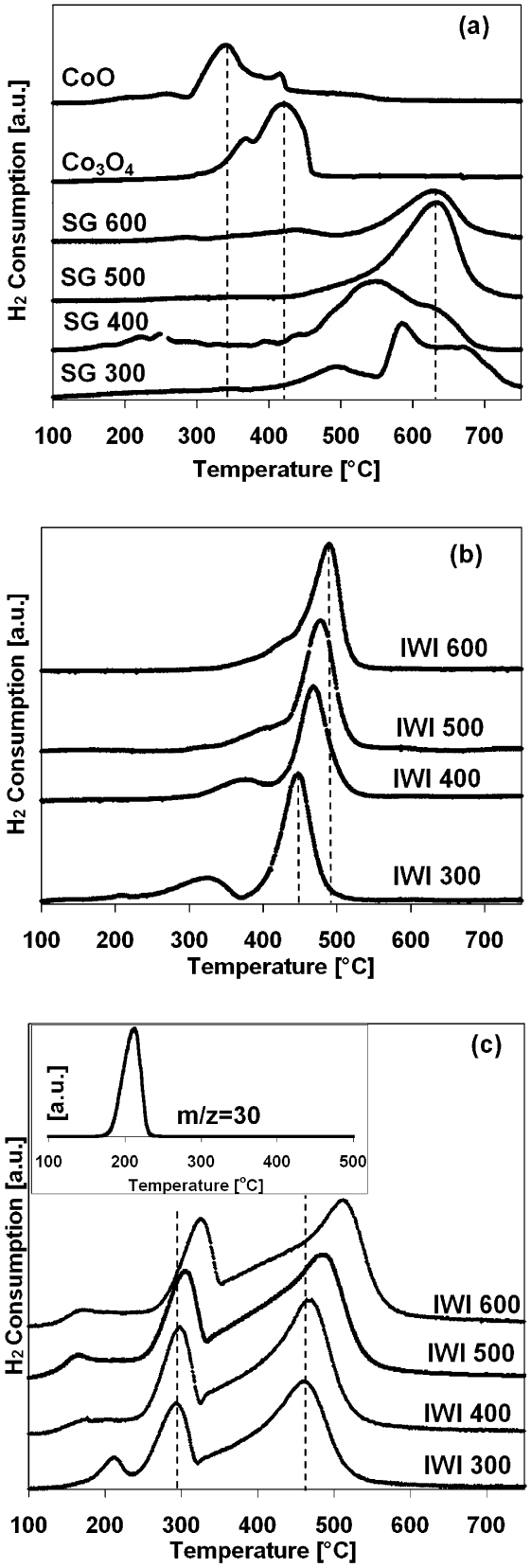

Fig. 4. Temperature-programmed reduction profiles of (a) reference materials and 10% Co/TiO_2 sol–gel catalysts calcined at various temperatures; (b) 10% Co/TiO_2 IWI catalysts calcined at various temperatures; and (c) 10% Co/ZrO_2 IWI catalysts calcined at various temperatures. Inset (c): Mass spectrometry signal of $m/z = 30$ during reduction of 10% Co/ZrO_2 IWI300.

700 and 750 °C. The broad reduction features indicate heterogeneity in the oxidation states and sites at which the cobalt species are located. The sol–gel preparation, which provides linkages between Ti and Co species, could partially account for this behavior. This heterogeneity was more pronounced in the SG300 sample. The 10% Co/TiO_2 sol–gel catalysts calcined at 500 and 600 °C showed better-defined reduction peaks at 625 °C. The high reduction temperatures indicate strong interaction with TiO_2 support.

Fig. 4b shows the TPR profiles for the 10% Co/TiO_2 IWI catalysts at various calcination temperatures. The 10% Co/TiO_2 IWI300 shows two distinct reduction peaks, around 330 and 450 °C, attributed to the Co^{3+} to Co^{2+} and Co^{2+} to Co^0 transitions, respectively [37,39,40,49–54]. In contrast to the Co/TiO_2 sol–gel catalysts, these reduction features are much sharper and better defined, indicating greater homogeneity among the types of supported cobalt species, and the lower reduction temperature indicates weaker interaction with the support matrix. With increasing catalyst calcination temperature, the position of the reduction peaks shifted to higher temperatures, due to any stronger metal–support interaction or sintering that might have occurred. With increasing calcination temperature, the high-temperature reduction peak shifted from 475 to 500 °C, and the low-temperature feature also shifted. In the IWI500 and IWI600 samples, this feature is just visible as a shoulder peak. The average Co oxidation states, determined using the hydrogen consumption values, for the Co/TiO_2 IWI samples were $Co^{2.59+}$, $Co^{2.56+}$, $Co^{2.57+}$, and $Co^{2.53+}$ for each of the four calcination temperatures (from lowest to highest, respectively). The average oxidation state of the Co_3O_4 reference material was calculated experimentally as $Co^{2.68+}$. The slight decrease in the average oxidation state with increasing calcination temperature may be due to the formation of a $CoTiO_3$ phase at higher calcination temperatures [42].

Fig. 4c shows the TPR profiles for 10% Co/ZrO_2 IWI calcined at different temperatures. Similar to the Co/TiO_2 samples, the reduction feature near 300 °C has been assigned to the transition from Co^{3+} to Co^{2+}, and the feature near 470 °C has been attributed to the reduction of Co^{2+} to Co^0 [37,39,40,49–52,54]. The small feature at around 200 °C can be attributed to the decomposition of nitrates that remained from the cobalt nitrate precursor used during the synthesis [49,55]. To help confirm this assignment, the effluent from a TPR experiment for 10% Co/ZrO_2 was monitored by mass spectrometry. The inset in Fig. 4c shows the mass spectrometry signal for the principle nitrate fragment, $m/z = 30$, during the TPR of 10% Co/ZrO_2 IWI300. The sharp peak at around 200 °C corresponds to the low-temperature feature observed in the TCD signal, which is attributed not to H_2 consumption, but rather to the change in thermal conductivity of the stream due to the presence of the nitrate species. The $m/z = 30$ signal for the samples calcined at higher temperatures during the TPR experiments (not shown) were substantially lower in intensity compared with those from the sample calcined at 300 °C. The ZrO_2-supported catalysts had a much more prominent low-temperature reduction feature (at around 300 °C) than the TiO_2-supported IWI catalysts. The hydrogen consumption represented by this low-

temperature peak agreed well with the theoretical hydrogen consumption for reduction of Co_3O_4 phase to CoO. The average oxidation state of Co on Co/ZrO_2 catalysts, after correction for the feature attributed to nitrates, was 2.69+ and did not change with increasing calcination temperature. In the activity measurement experiments, the 10% Co/ZrO_2 catalysts were less sensitive to calcination temperature than the Co/TiO_2 catalysts. The shift in the reduction temperatures was not as pronounced over the ZrO_2-supported catalysts, and the reduction temperatures were lower than for the TiO_2-supported ones. These observations may suggest stronger interaction of the Co with the titania support and easier accessibility of oxygen on the zirconia-supported catalyst. TPR of various Co/ZrO_2 IWI300 metal loadings (5, 10, and 15%) were examined (data not shown) and showed similar reduction peak profiles and temperatures, indicating that similar species were present at each loading level. TPR experiments on the unloaded TiO_2 and ZrO_2 supports were also conducted and did not show any reduction features.

3.3. XRD

During the calcination of the catalysts, in situ XRD was performed to examine changes in both the Co and support crystal structure. The diffraction patterns during these experiments for the 10% Co catalysts on TiO_2 and ZrO_2, prepared via both IWI and sol–gel, are shown in Figs. 5 and 6. The Co/TiO_2 IWI catalyst, Fig. 5a, showed only anatase TiO_2 up until 600 °C, as indicated by the [101], [103], [004], and [112] diffraction lines at 2θ values of 25.3°, 36.9°, 37.7°, and 38.6°, respectively. A narrowing of these peaks indicates the development of increased crystallinity. The new phase appearing at 700 °C is due to $CoTiO_3$, with [012], [104], [110], and [113] diffraction lines at respective 2θ values of 24.0°, 33.0°, 35.3°, and 40.4°. At 750 °C, a phase change in the TiO_2 is observed, with the formation of rutile TiO_2 as indicated by the [110], [101], and [111] diffraction lines at 2θ values of 27.4°, 36.0°, and 41.2°.

The diffraction patterns in Fig. 5b for 10% Co/TiO_2 sol–gel show different transformation behaviors than the catalyst prepared by IWI. At 300 °C, no crystalline phases were observed, but broad peaks associated with anatase TiO_2 appeared at 400 °C. At 500 °C, the sharpening of the anatase TiO_2 peaks is accompanied by the appearance of $CoTiO_3$, as indicated by the previously mentioned diffraction lines. At 600 °C, the diffraction lines from rutile TiO_2 appeared and grew with increasing temperature, whereas the intensity of the anatase TiO_2 diffraction lines decreased. The diffraction lines at 2θ values of 34.9°, 37.5°, and 43.1° are due to the Al_2O_3 sample holder. Crystalline Co or Co-oxide phases were not detected through XRD in either the sol–gel or the IWI preparation. Note, however, that $CoTiO_3$ was detected at lower temperatures on the Co/TiO_2 SG sample compared with the IWI sample (500 vs 700 °C). The formation of the $CoTiO_3$, then, corresponds to the decrease in NO oxidation activity with increasing calcination temperature that was observed on these samples and also helps explain why the sol–gel-prepared samples showed a greater loss

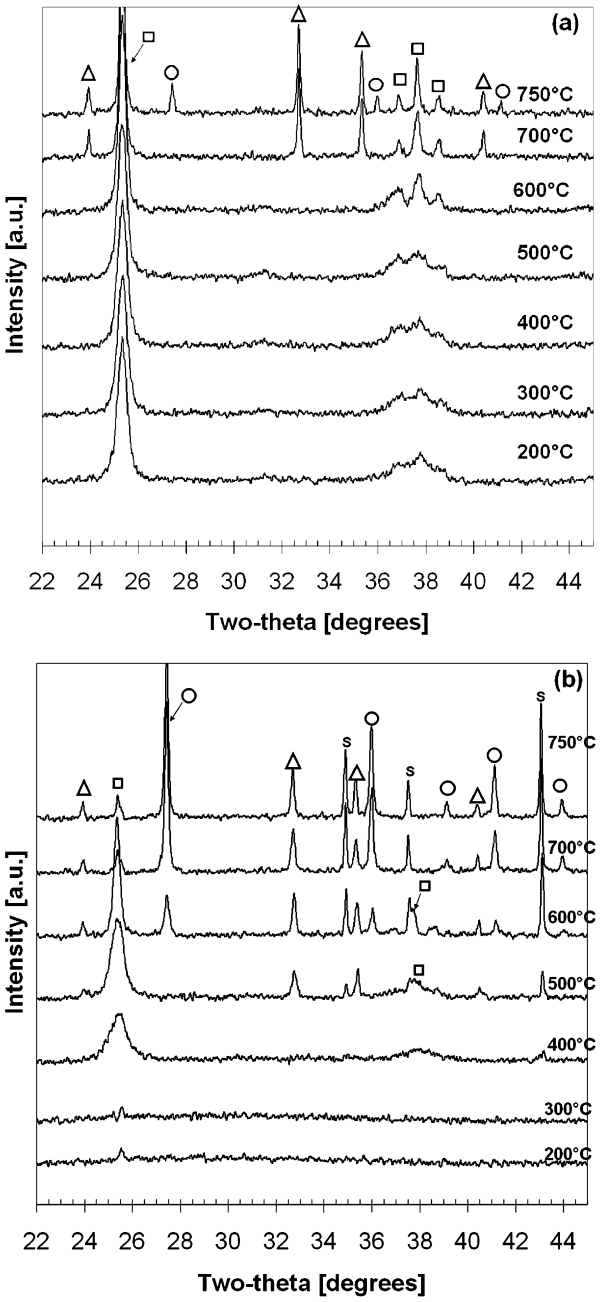

Fig. 5. In situ XRD patterns during the calcination of (a) 10% Co/TiO_2 IWI; (b) 10% Co/TiO_2 sol–gel. Anatase TiO_2 (□), rutile TiO_2 (○), $CoTiO_3$ (△), and Al_2O_3 sample holder (S).

in activity than the IWI samples with increasing annealing temperature.

The calcination experiments monitored by in situ XRD for 10% Co/ZrO_2 IWI and 10% Co/ZrO_2 SG are shown in Figs. 6a and 6b, respectively. Fig. 6a shows that the IWI support is monoclinic ZrO_2 as indicated by the [-111], [111], and [-112] diffraction lines appearing at 28.5°, 31.5°, and 40.7° 2θ values, which remain stable throughout the calcination. With a temperature increase from 100 to 800 °C, crystalline Co_3O_4 particles increased in size, as indicated by sharpening of the [311], [222], and [400] diffraction lines located at 2θ values of 36.9°, 38.6°, and 44.9° in Fig. 6a.

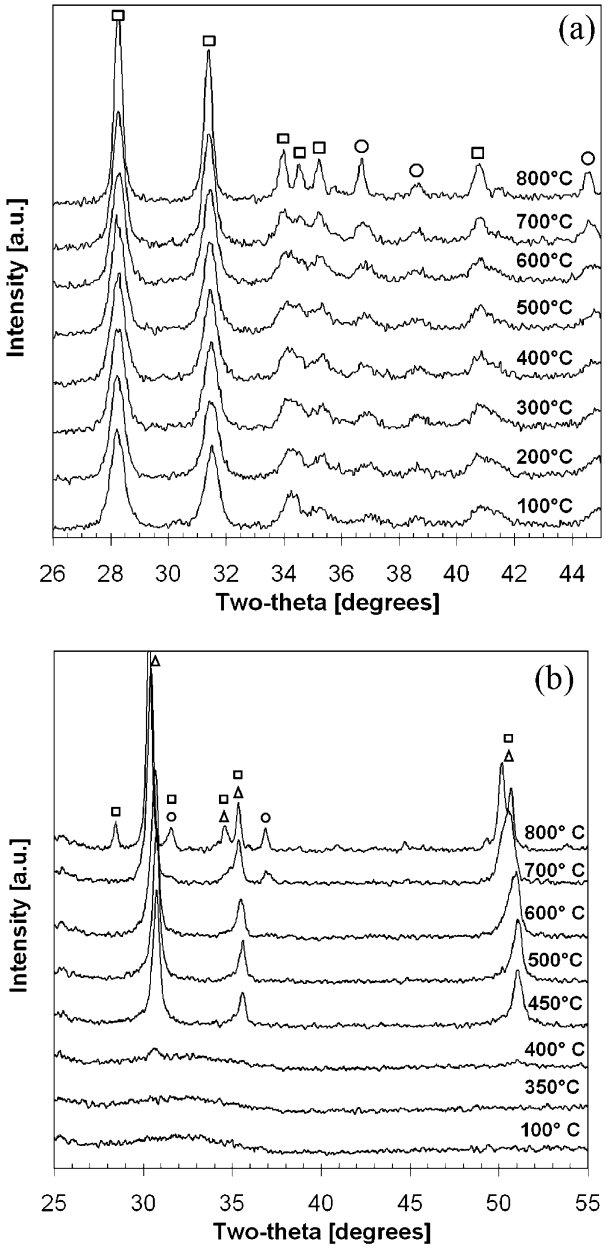

Fig. 6. In situ XRD patterns during the calcination of (a) 10% Co/ZrO_2 IWI; (b) 10% Co/ZrO_2 sol–gel. Monoclinic ZrO_2 (□), Co_3O_4 (○), and tetragonal ZrO_2 (△).

The in situ XRD patterns acquired during calcination of 10% Co/ZrO_2 sol–gel, shown in Fig. 6b, reveal that the material was amorphous until around 450 °C, at which point tetragonal ZrO_2 began to form. The appearance of [101] and [200] diffraction lines around 2θ values of 31° and 50° was due to a shift from tetragonal ZrO_2 toward monoclinic ZrO_2, which did not begin to prominently appear until 800 °C. The [311] diffraction line at 36.9° due to crystalline Co_3O_4 appeared at 700 °C. It is interesting to note the Co_3O_4 was observed at lower temperature on Co/ZrO_2 IWI than on Co/ZrO_2 sol–gel. This may be related to the ability of crystalline cobalt oxide clusters to form without significant interactions with the support on the Co/ZrO_2 IWI catalyst.

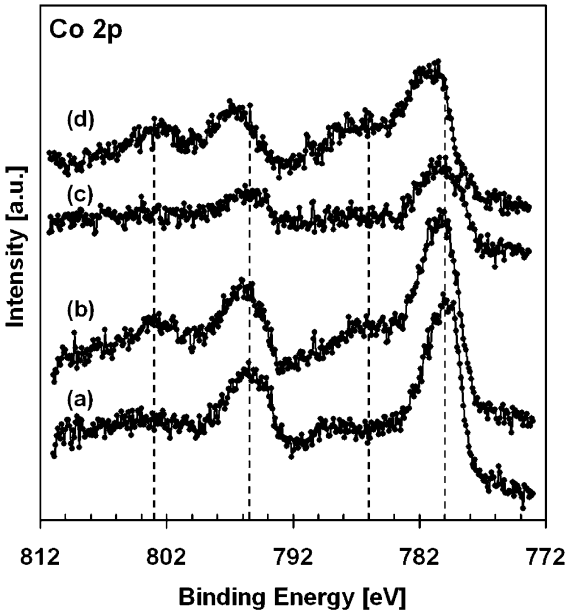

Fig. 7. XPS spectra of Co 2p region of (a) 10% Co/ZrO_2 IWI300, (b) partially reduced 10% Co/ZrO_2 IWI300, (c) 10% Co/TiO_2 IWI300, and (d) partially reduced 10% Co/TiO_2 IWI300.

3.4. XPS

The Co/TiO_2 and Co/ZrO_2 IWI catalysts were also characterized using XPS. Spectra of the Co 2p, Zr 3d, Ti 2p, O 1s, and C 1s regions were collected. For all of the spectra collected, the binding energies of the Ti 2p, Zr 3d, and O 1s peaks were typical of the TiO_2 or ZrO_2 support. Spectra of 1, 5, 8, 10, 12, and 15 wt% Co/ZrO_2 IWI 300 were collected. The Co 2p regions differed only in intensity, not in binding energy. 10% Co/ZrO_2 samples calcined at 300, 400, 500, and 600 °C were also examined. The Co 2p regions at the various calcination temperatures had peaks at the same binding energy and nearly identical intensities. The two characteristic peaks of Zr 3d remained stable for all calcination temperatures, showing no significant change in the monoclinic ZrO_2 support at the different temperatures [56,57]. For the Co/ZrO_2 samples with varying metal loadings and calcination temperatures, the Co $2p_{3/2}$ and Co $2p_{1/2}$ binding energy values were consistent with the presence of both Co^{3+} and Co^{2+}, which differ from each other by 0.9 eV, with Co^{2+} at the higher binding energy [58,59]. The distinguishing features used to differentiate between Co^{3+} and Co^{2+} are shake-up peaks located at about 6 eV higher binding energy from the main Co 2p peaks [58,59]. Clear shake-up peaks were not observed, indicating that a significant amount of cobalt was in the Co^{3+} oxidation state, consistent with the presence of Co_3O_4 in which 2/3 of the cobalt is in the Co^{3+} oxidation state. The absence of clear shake-up peaks on samples containing 10% Co is not surprising since even the shake-up peaks observed from bulk Co_3O_4 were relatively weak [53,54,60].

XPS spectra of 10% Co/TiO_2 IWI300 and 10% Co/ZrO_2 IWI300 taken of the as-prepared samples and after a partial reduction are shown in Fig. 7. The partially reduced samples were treated in the same manner as described in the TPR section. However, instead of continuing the temperature program up to

800 °C, the H_2 flow was immediately stopped after the first reduction features had ended (325 °C for Co/ZrO_2 and 375 °C for Co/TiO_2), and the samples were cooled in N_2 and transferred for XPS analysis without being exposed to air. Spectra (a) and (c) of the as-prepared samples showed the Co $2p_{3/2}$ peak maximum at 779.7 eV on Co/ZrO_2 and at 780.4 eV on Co/TiO_2, which can be attributed to a greater percentage of surface cobalt being in the Co^{3+} oxidation state on ZrO_2 compared with TiO_2. The shake-up peaks that are indicative of Co^{2+} were not readily observed. The partially reduced samples shown in (b) and (d) exhibit the shake-up features at 6 eV higher binding energy, indicating that Co_3O_4 has been reduced to Co^{2+}. A slight shift toward higher binding energy in the main Co 2p peaks also can be seen, consistent with the reduction of Co^{3+} to Co^{2+}. These observations are agreement with the TPR data, which show that the first reduction feature corresponds to the reduction of Co_3O_4 phase to CoO phase. The lower binding energy observed over the ZrO_2-supported sample is also consistent with the higher average oxidation state calculated for this sample using the hydrogen consumption in TPR experiments.

3.5. Laser Raman spectroscopy

Fig. 8 shows the laser Raman spectra taken over the impregnated 10% Co/ZrO_2 and 10% Co/TiO_2 catalysts at various calcination temperatures, along with reference spectra taken over unloaded TiO_2, unloaded ZrO_2, and bulk Co_3O_4. The ZrO_2 support showed strong Raman bands at 179, 192, 335, 385, 478, 619, and 640 cm^{-1} which are typical of monoclinic ZrO_2 [42,48,61]. The bands at 193, 475, 516, 615, and 680 cm^{-1} have previously been attributed to Co_3O_4 [42–44,62]. The spectra of the 10% Co/ZrO_2 samples are almost identical to that obtained from the bulk Co_3O_4, whereas the vibrational bands that correspond to the ZrO_2 support are barely visible. This is likely due to the smaller Raman cross-section of m-ZrO_2 compared with Co_3O_4 [63].

The TiO_2 bands at 142, 197, 396, 516, and 639 cm^{-1} are typical of anatase TiO_2 [42–44]. For the Co/TiO_2 catalysts, the TiO_2 bands were visible at all calcination temperatures, and the Co_3O_4 bands were less pronounced than on the ZrO_2 support. The bands at 479 and 683 cm^{-1} associated with Co_3O_4 were clearly visible at 500 and 600 °C. The broadening of the TiO_2 bands may be attributed to interactions with cobalt species and disorder in the oxygen sublattice [64]. The lack of Co_3O_4 Raman bands at lower calcination temperatures on the TiO_2-supported samples suggests that Co_3O_4 does not form as readily on the surface compared with the ZrO_2 support [42]. This difference in surface Co_3O_4 is likely related to the differences in NO oxidation activity observed over the TiO_2 and ZrO_2 catalysts.

3.6. DRIFTS on 10% Co/ZrO_2

NO adsorption was performed on 10% Co/ZrO_2 IWI500 catalyst, and the DRIFTS spectra were obtained as temperature was increased; these are displayed in Fig. 9a. A broad band between 3600 and 3000 cm^{-1} was observed that can be attributed to H-bonded hydroxyl groups [65]. The intensity of the hydroxyl group band decreased with increasing temperature and disappeared by 300 °C. The bands at 1620, 1233, and 1004 cm^{-1} have been assigned to bridging nitrates [66,67]. The bridging nitrate intensities decreased with increasing temperature, but a band at 1233 cm^{-1} was still clearly present at 350 °C. The bands at 1588, 1560, 1240, and 1040 cm^{-1} are typical of bidentate nitrates [66,68]. The band at 1505 cm^{-1} is assigned to monodentate nitrates [66,69]; the band at 1302 cm^{-1} is associated with metal-bonded nitro species [66,69]. These nitro groups begin to disappear at 150 °C and are essentially re-

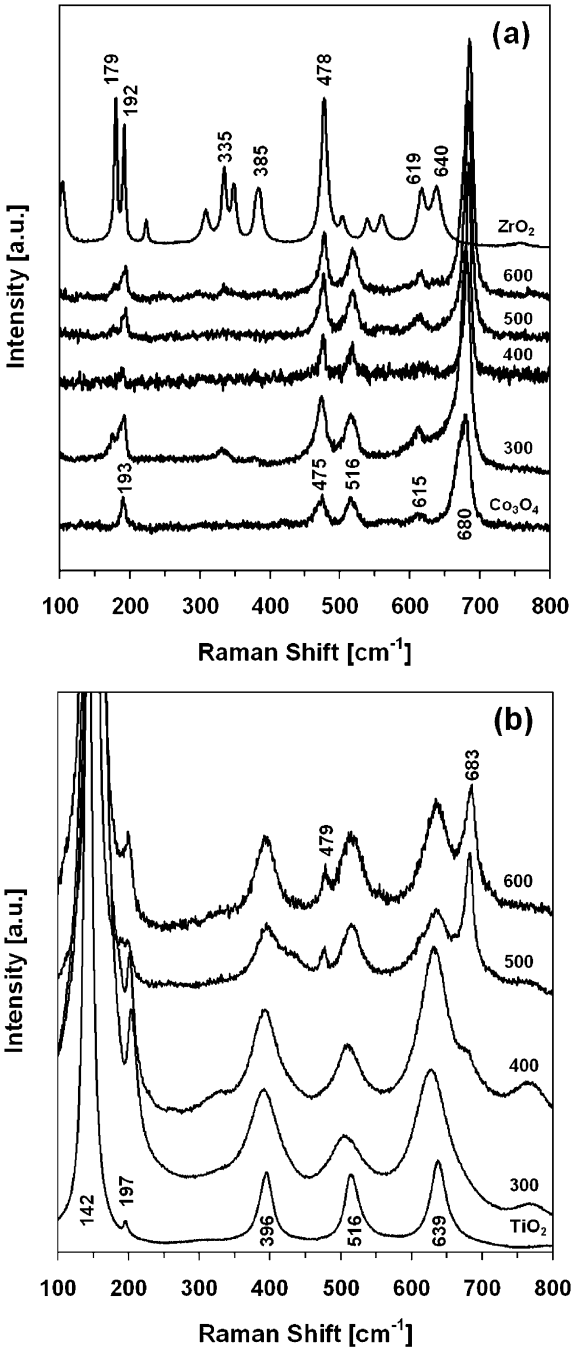

Fig. 8. Laser Raman spectra of reference materials and 10% Co samples at various calcination temperatures supported on (a) ZrO_2 and (b) TiO_2.

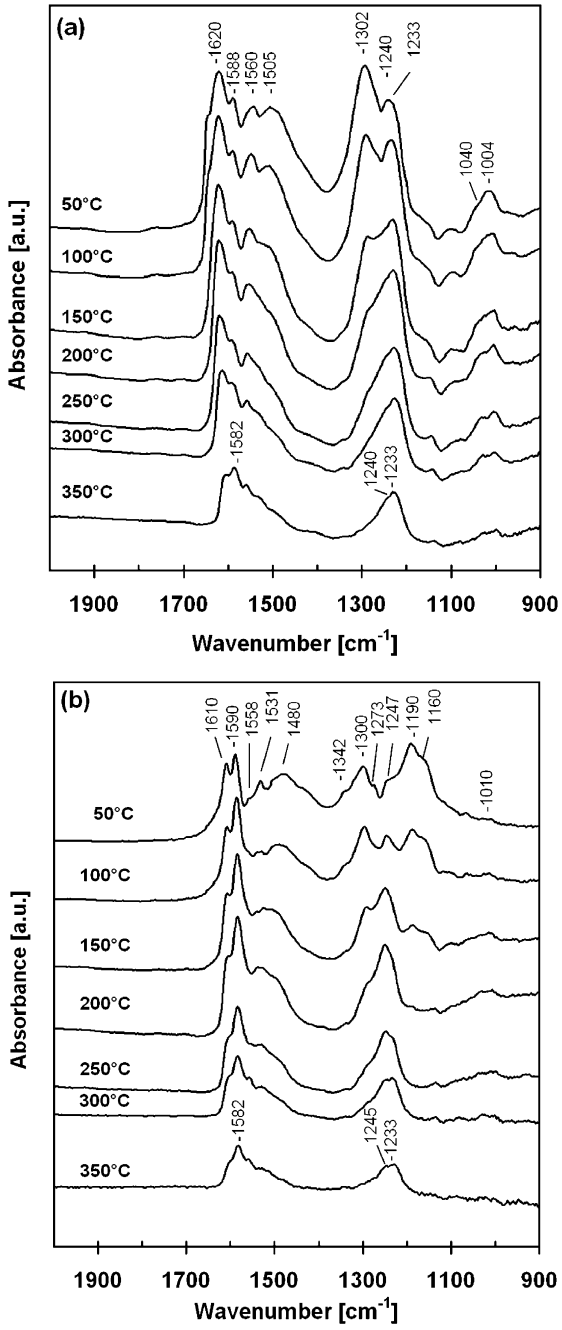

Fig. 9. DRIFTS spectra on 10% Co/ZrO_2 after (a) NO or (b) NO_2 adsorption.

moved by 300 °C. Even after the temperature reached 350 °C, the bands at 1582 and 1233 cm^{-1}, typical of the bidentate and bridging nitrates, remained. The loss of intensity for the monodentate nitrate surface species while the bidentate and bridging nitrate species remain at 350 °C is consistent with their relative stability, bridging nitrates > bidentate nitrates > monodentate nitrates [67].

The DRIFTS spectra for the NO_2 adsorption on 10% Co/ZrO_2 IWI500 are shown in Fig. 9b. A broad band associated with hydroxyl groups was once again found in the 3600–3000 cm^{-1} region, but it disappeared by 300 °C. Multiple bands were present at 50 °C, but all except those typical of bidentate and bridging nitrates essentially disappeared by 350 °C. The

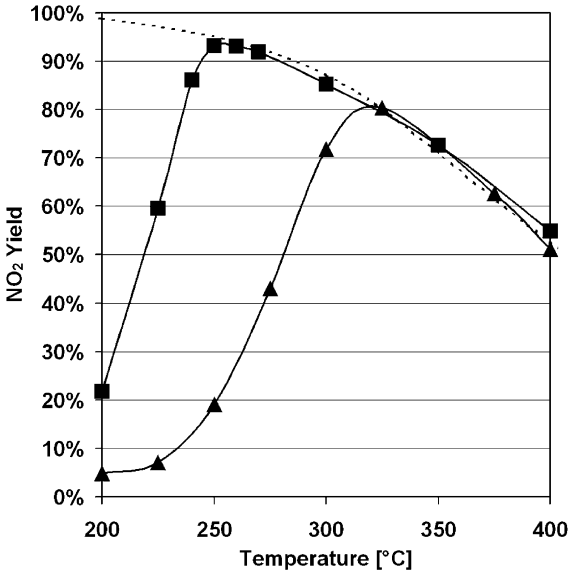

Fig. 10. NO oxidation activity on (■) 10% Co/ZrO_2 IWI300 and (▲) unsupported Co_3O_4 based on equal cobalt mass.

bands at 1610 and 1010 cm^{-1} are attributed to cobalt-bound monodentate nitrites [67,69]. The band at 1342 cm^{-1} can be attributed to either monodentate nitrite species or nitro compounds [67,69]. Bidentate nitrates are responsible for the bands at 1590, 1558, and 1190 cm^{-1} [65,66,68,70]. Monodentate nitrates are responsible for the bands at 1531 and 1480 cm^{-1} [67,69]. Adsorbed nitro species result in the bands at 1300, 1273, and 1247 cm^{-1} [66,67,69]. The band at 1160 cm^{-1} arises from the ν(N–O) [67]. The intensities of the bands at 1590 and 1247 cm^{-1} increase up to 200 °C, after which their intensity begins to diminish. At temperatures below 300 °C, there are some differences in the types of surface species found on 10% Co/ZrO_2 after the adsorption of either NO or NO_2. At temperatures of 300 °C and above, however, surface transformations give rise to the same types of surface species on the Co/ZrO_2 catalyst after the NO or NO_2 adsorption.

3.7. Steady-state reaction on unsupported Co_3O_4

The NO oxidation activity of unsupported Co_3O_4 was also tested; it is compared with the most active supported catalyst from this study, 10% Co/ZrO_2 IWI300, in Fig. 10. Experiments were conducted on basis of equal cobalt mass (20 mg). The results indicate that bulk Co_3O_4 was active for the NO oxidation reaction, reaching the thermodynamic equilibrium at 325 °C. The higher activity observed on the Co/ZrO_2 catalyst may be attributed to the high surface area of the support. This indicates that a high-surface area support that provides good dispersion of Co_3O_4 particles would be highly active for the oxidation of NO to NO_2 in excess oxygen.

4. Conclusion

Cobalt catalysts supported on TiO_2 and ZrO_2 were prepared by sol–gel and IWI techniques and evaluated for their activity for NO oxidation to NO_2 in excess O_2. The activity was

found to be a strong function of the support, preparation technique and the pretreatment conditions. The Co/ZrO_2 catalysts prepared by IWI had the highest NO chemisorption uptake per unit surface area. It appears that the zirconia support not only leads to a better catalyst dispersion and a higher site density on the surface compared with TiO_2, but also provides better intrinsic activity. Although the results presented in this article are not sufficient to provide a basis for determining the cause of these intrinsic activity differences, possibility causes include involvement of the support in the oxygen-insertion step and differences in Co_3O_4 particle size or orientation. Co/ZrO_2 catalysts appear to be promising candidates for NO oxidation in a dual-catalyst scheme in which NO is first oxidized to NO_2 and then NO_2 is subsequently reduced to N_2 with a hydrocarbon under lean conditions.

Acknowledgments

Funding for this work was provided by the United States Department of Energy (DOE) and the National Energy Technology Laboratory (NETL) through cooperative agreement DE-FC26-02NT41610, as well as the National Science Foundation through NSF-DMR grant 0114098.

References

[1] A. Konig, W. Held, T. Ricker, Top. Catal. 28 (2004) 99.
[2] E. Hums, Catal. Today 42 (1998) 25.
[3] P. Vernoux, A.-Y. Leinekugel-Le-Cocqu, F. Gaillard, J. Catal. 219 (2003) 247.
[4] S. Mendioriz, A.B. Martin-Rojo, F. Rivera, J.C. Martin, A. Bahamonde, M. Yates, Appl. Catal. B 64 (2006) 161.
[5] J.-Y. Yan, H.H. Kung, W.M.H. Sachtler, M.C. Kung, J. Catal. 175 (1998) 294.
[6] M.C. Kung, H.H. Kung, Top. Catal. 28 (2004) 105.
[7] M.D. Amiridis, T. Zhang, R.J. Farrauto, Appl. Catal. B 10 (1996) 203.
[8] M. Iwamoto, H. Yahiro, Catal. Today 22 (1994) 5.
[9] S. Sato, H. Hirabayashi, H. Yahiro, N. Mizuno, M. Iwamoto, Catal. Lett. 12 (1992) 193.
[10] H.K. Shin, H. Hirabayashi, H. Yahiro, M. Watanabe, M. Iwamoto, Catal. Today 26 (1995) 13.
[11] Y. Li, J.N. Armor, Appl. Catal. B 1 (1992) L31.
[12] Y. Li, J.N. Armor, J. Catal. 145 (1994) 1.
[13] C. Yokoyama, M. Misono, Chem. Lett. (1992) 1669.
[14] H. Hamada, Y. Kintaichi, M. Sasaki, T. Ito, M. Tabata, Appl. Catal. 70 (1991) L15.
[15] Y. Li, P.J. Battavio, J.N. Armor, J. Catal. 142 (1993) 561.
[16] X. Zhang, A.B. Walter, M.A. Vannice, Appl. Catal. B 4 (1994) 237.
[17] R. Burch, J.P. Breen, F.C. Meunier, Appl. Catal. B 39 (2002) 283.
[18] R. Burch, A. Ramli, Appl. Catal. B 15 (1998) 49.
[19] R. Burch, A. Ramli, Appl. Catal. B 15 (1998) 63.
[20] M.J. Castagnola, M.K. Neylon, C.L. Marshall, Catal. Today 96 (2004) 61.
[21] J.R. Regalbuto, T. Zheng, J.T. Miller, Catal. Today 54 (1999) 495.
[22] J. Despres, M. Elsener, M. Koebel, O. Krocher, B. Schnyder, A. Wokaun, Appl. Catal. B 50 (2004) 73.
[23] F.C. Meunier, J.R.H. Ross, Appl. Catal. B 24 (2000) 23.
[24] H. Ohtsuka, Appl. Catal. B 33 (2001) 325.
[25] S. Bennici, A. Gervasini, Appl. Catal. B 62 (2006) 336.
[26] J.O. Petunchi, W.K. Hall, Appl. Catal. B 2 (1993) L17.
[27] A.Yu. Stakheev, C.W. Lee, S.J. Park, P.J. Chong, Catal. Lett. 38 (1996) 271.
[28] A.Yu. Stakheev, C.W. Lee, S.J. Park, P.J. Chong, Appl. Catal. B 9 (1996) 65.
[29] P.W. Park, C.S. Ragle, C.L. Boyer, M.L. Balmer, M. Engelhard, D. McCready, J. Catal. 210 (2002) 97.
[30] M.K. Neylon, M.J. Castagnola, N.B. Castagnola, C.L. Marshall, Catal. Today 96 (2004) 53.
[31] S.N. Orlik, V.L. Struzhko, T.V. Mironyuk, V.P. Kazimirov, Theor. Exp. Chem. 39 (2003) 184.
[32] C.M. de Correa, A.L. Villa de P., Catal. Lett. 53 (1998) 205.
[33] K.A. Bethke, H.H. Kung, J. Catal. (1997) 93.
[34] N. Bogdanchikova, F.C. Meunier, M. Avalos-Borja, J.P. Breen, A. Pestryakov, Appl. Catal. B 36 (2002) 287.
[35] E. Xue, K. Seshan, J.R.H. Ross, Appl. Catal. B 11 (1996) 65.
[36] G. Jacobs, T.K. Das, Y. Zhang, J. Li, G. Racoillet, B.H. Davis, Appl. Catal. A 233 (2002) 263.
[37] P.A. Chernavskii, A.S. Lermontov, G.V. Pankina, S.N. Torbin, V.V. Lunin, Kinet. Catal. 43 (2002) 292.
[38] J.-S. Girardon, A. Constant-Griboval, L. Gengembre, P.A. Chernavskii, A.Y. Khodakov, Catal. Today 106 (2005) 161.
[39] S. Sun, K. Tsubaki, K. Fujimoto, Appl. Catal. A 202 (2000) 121.
[40] M.J. Tiernan, E.A. Fesenko, P.A. Barnes, G.M.B. Parkes, M. Ronane, Thermochim. Acta 379 (2001) 163.
[41] F. Wyrwalski, J.-F. Lamonier, M.J. Perez-Zurita, S. Siffert, A. Aboukaïs, Catal. Lett. 108 (1–2) (2006) 87.
[42] T. Xiao, S.J. Ji, H. Wang, K.S. Coleman, M.L.H. Green, J. Mol. Catal. A 175 (2001) 111.
[43] Y. Brik, M. Kacimi, M. Ziyad, F. Bozon-Verduraz, J. Catal. 202 (2001) 118.
[44] Y. Brik, M. Kacimi, F. Bozon-Verduraz, M. Ziyad, J. Catal. 211 (2002) 470.
[45] E.M. Holmgreen, M.M. Yung, U.S. Ozkan, Proceedings of ICEF04 ASME 2004 Fall Technical Conference, vol. 893, 2004, p. 1.
[46] E.M. Holmgreen, M.M. Yung, U.S. Ozkan, Catal. Lett. 111 (1–2) (2006) 19.
[47] E.M. Holmgreen, M.M. Yung, U.S. Ozkan, Appl. Catal. B Environ. (2007), doi:10.1016/j.apcatb.2007.01.012, in press.
[48] E.M. Holmgreen, M.M. Yung, U.S. Ozkan, J. Mol. Catal. A Chem. (2007), doi:10.1016/j.molcata.2007.01.030, in press.
[49] A.R. Belambe, R. Oukaci, J.G. Goodwin Jr., J. Catal. 166 (1997) 8.
[50] C.L. Bianchi, Catal. Lett. 76 (2001) 155.
[51] Y. Zhang, D. Wei, S. Hammache, J.G. Goodwin Jr., J. Catal. 188 (1999) 281.
[52] N.N. Madikizela-Mnqanqeni, N.J. Coville, J. Mol. Catal. A 225 (2005) 137.
[53] F.B. Noronha, C.A. Perez, M. Schmal, R. Frety, Phys. Chem. Chem. Phys. 1 (1999) 2861.
[54] M. Haneda, Y. Kintaichi, N. Bion, H. Hamada, Appl. Catal. B 46 (2003) 473.
[55] H.K. Lin, H.C. Chui, H.C. Tsai, S.H. Chien, Catal. Lett. 88 (2003) 169.
[56] V. Quaschning, J. Deutsch, P. Druska, H.-J. Niclas, E. Kemnitz, J. Catal. 177 (1998) 164.
[57] H.C. Zeng, J. Lin, W.K. Teo, F.C. Loh, K.L. Tan, J. Non-Cryst. Solids 181 (1995) 49.
[58] D. Pietrogiacomi, S. Tuti, M.C. Campa, V. Indovina, Appl. Catal. B 28 (2000) 43.
[59] W.S. Epling, G.B. Hoflund, J.F. Weaver, J. Phys. Chem. 100 (1996) 9929.
[60] L.F. Liotta, G. Di Carlo, G. Pantaleo, A.M. Venezia, G. Deganello, Appl. Catal. B 66 (2006) 217–227.
[61] C. Li, M. Li, J. Raman Spectrosc. 33 (2002) 301.
[62] H. Ohtsuka, T. Tabata, O. Okada, L.M.F. Sabatino, G. Bellussi, Catal. Lett. 44 (1997) 265.
[63] A. Gajovic, I. Djerdj, K. Furic, R. Schlogl, D.S. Su, Cryst. Res. Technol. 41 (2006) 1076.
[64] J. Cai, C. Raptis, Y.S. Raptis, E. Anastassakis, Phys. Rev. B 51 (1995) 201.
[65] M. Kantcheva, A.S. Vakkasoglu, J. Catal. 223 (2004) 352.
[66] K. Hadjiivanov, V. Avreyska, D. Klissurski, T. Marinova, Langmuir 18 (2002) 1619.

[67] K.I. Hadjiivanov, Catal. Rev. Sci. Eng. 42 (2000) 71.
[68] B. Tsyntsarski, V. Avreyska, H. Kolev, Ts. Marinova, D. Klissurski, K. Hadjiivanov, J. Mol. Catal. A 193 (2003) 139.
[69] V.A. Sadkykov, V.V. Lunin, V.A. Matyshak, E.A. Paukshtis, A.Ya. Rozovskii, N.N. Bulgakov, J.R.H. Ross, Kinet. Catal. 44 (2003) 379.
[70] M. Kantcheva, A.S. Vakkasoglu, J. Catal. 223 (2004) 364.